Comparative Study on the Performance and Hydration Mechanism of Coal Gangue Cementitious Materials with Different Alkali Activators

Chao Geng , Yajie Gao , Quanming Li * , Zongyuan Mao , Xianfeng Shi , Wei Li , Yajie Wang , Cheng Chen , Yukai Wang

Posted Date: 3 February 2026

doi: 10.20944/preprints202602.0215.v1

Keywords: CG; alkali activator; cementitious properties; N-A-S-H gel; hydration mechanism; resource utilization

Article

Comparative Study on the Performance and Hydration Mechanism of Coal Gangue Cementitious Materials with Different Alkali Activators

Chao Geng [1], Yajie Gao [1], Quanming Li [1,*], Zongyuan Mao [2], Xianfeng Shi [3], Wei Li [1], Yajie Wang [1], Cheng Chen [1,4] and Yukai Wang [1,4]

[1] School of Civil Engineering, North China University of Technology, Beijing 100144, China
[2] China Academy of Building Research, Beijing 100013, China
[3] School of Mine Safety, University of Emergency Management, Hebei, Langfang 065201, China.
[4] Key Laboratory of Disaster Prevention and Control Technology and Equipment for Tailings Ponds, State Administration of Mining Safety, China
* Correspondence: liqm@ncut.edu.cn

Abstract

Coal gangue (CG) is one of ranks among China's most significant industrial by-products. In response to China's carbon neutrality commitments and the growing emphasis on resource recycling, finding effective ways to valorize CG has emerged as a pressing concern. Based on the mineral composition and chemical composition characteristics of CG, this study systematically investigated the enhancement effects of three alkali activators (sodium silicate, NaOH, and $Ca(OH)_2$) on the cementitious properties of CG. Through different dosage and compressive strength tests, the efficiency ranking of the three activators was determined as: sodium silicate > $Ca(OH)_2$ > NaOH. A 10% sodium silicate dosage combined with 28-day curing was identified as the optimal condition for achieving sufficient reaction and structural densification. Under these conditions, the compressive strength of CG cementitious material reached 6.4 MPa, representing an increase of 190.9% compared to the blank group (2.2 MPa), significantly superior to $Ca(OH)_2$ (69.55%) and NaOH (62.27%). X-ray diffraction (XRD) and scanning electron microscopy-energy dispersive spectroscopy (SEM-EDS) analyses revealed thatalkali activators function primarily by disrupting the crystalline framework of CG, promote the cross-linking polymerization of silicon-aluminum monomers to generate dense cementitious products, thereby improving material performance. The sodium silicate is attributed to its "dual activation effect", providing OH^- to create an alkaline environment while supplying reactive silicate ions (SiO_3^{2-}) to accelerate N-A-S-H gel and C-A-S-H gel formation. These findings offer guidance for optimizing CG-based cementitious formulations for the formula optimization and large-scale utilization of CG cementitious materials.

Keywords: CG; alkali activator; cementitious properties; N-A-S-H gel; hydration mechanism; resource utilization

1. Introduction

Coal continues to dominate China's energy mix, coal accounted for 66.6% of the energy production structure in 2023. By the end of 2023, China's coal reserves reached 218.57 billion tons, and raw coal production reached 4.76 billion tons in 2024, setting a historical record [1]. Intensive coal extraction has led to steadily rising CG output, showing an overall upward trend from 2011 to 2022, mainly distributed in major coal-producing areas such as Shanxi, Inner Mongolia, and Shaanxi provinces. Currently, China has formed more than 2,700 gangue mountains, with a total stockpile exceeding 7 billion tons, occupying more than 200,000 mu of land, establishing CG as a major

 doi:10.20944/preprints202602.0215.v1

contributor to China's industrial waste burden[2,3]. During the stockpiling process, the heavy metals and acidic substances contained in CG can easily infiltrate underground through rainwater erosion, polluting water resources and soil. Meanwhile, the loose mountain structure poses collapse risks, threatening the surrounding ecological environment and human safety [4].

To promote the resource utilization of CG, China has successively issued policies such as the "Administrative Measures for Comprehensive Utilization of CG" and "Opinions on Strengthening Clean and Efficient Utilization of Coal", explicitly proposing to advance CG utilization in ecological restoration, backfilling mining, and engineering construction. CG is rich in minerals such as kaolinite and quartz , as well as chemical components like Al_2O_3 and SiO_2, possessing the potential for transformation into resource products such as cementitious materials and adsorbent materials [5,6]. However, its low natural reactivity limits high-value utilization efficiency, making activation technology to enhance its performance a key research direction [7–10].

Alkali-activated materials (AAMs) are novel cementitious materials prepared using industrial solid wastes as raw materials and alkaline solutions as activators, with advantages of low carbon footprint, environmental friendliness, and excellent mechanical properties [11,12]. Common alkali activators include sodium hydroxide, calcium hydroxide, sodium silicate, and their composite systems. Provis et al. [13] Provided a comprehensive overview of how alkali-activated materials undergo hydration, noting that elevated pH conditions facilitate Al-O and Si-O bond cleavage in raw materials, liberating soluble silicate and aluminate species that polymerize into interconnected gel networks of N-A-S-H or C-A-S-H gels. Zhou et al. [7] reported a strong dependence of material performance on sodium silicate modulus of alkali-activated materials, with an appropriate modulus promoting gel product formation and optimizing microstructure. Wang et al. [8] examined how different activator chemistries govern mechanical behavior of CG geopolymers, indicating that the activator type is a decisive factor; Feng et al. [9] explored the sustainable alkali-activation application of spontaneous combustion CG, emphasizing the importance of raw material characteristics. However, existing research mostly adopts CG-slag/fly ash blended systems [14], and systematic comparative studies of pure CG systems under identical conditions are relatively lacking. Although certain progress has been made in CG alkali-activated materials research, the following shortcomings remain: (1) most studies focus on single activator systems, lacking systematic comparisons of different activator types under identical conditions; (2) activation mechanism research is insufficient, particularly regarding the advantage mechanisms of sodium silicate compared to NaOH and $Ca(OH)_2$, which have not been fully elucidated.

To address the above issues, this study uses CG from Taiyuan, Shanxi as raw material, systematically comparing the effects of sodium silicate, NaOH, and $Ca(OH)_2$ under identical conditions on the cementitious properties of CG, combined with XRD, SEM-EDS, and other micro-characterization methods to reveal the activation mechanism.

2. Materials and Methods

2.1. Experimental Materials

2.1.1. Coal Gangue

CG constitutes the lithic fraction discarded throughout coal extraction and processing operations, predominantly comprising mineral assemblages including kaolinite, mica, and quartz. The CG specimens investigated herein were sourced from a Taiyuan-based colliery, Shanxi, subjected to jaw crushing followed by ball milling for 2 h before sieving. The elemental oxide distribution is presented in Table 1. It can be seen that the main chemical components of CG are SiO_2, Al_2O_3, and Fe_2O_3, with a silicon-aluminum ratio (SiO_2/Al_2O_3) of 2.73. The XRD pattern shown in Figure 1(a) indicates that the main minerals in this CG are quartz, mica, calcite, and kaolinite, demonstrating its potential as a precursor for alkali-activated materials [15]. The micromorphology shown in Figure 1(b) reveals that CG consists of loose particles without agglomeration.

Table 1. Main chemical composition of CG samples.

Component	SiO_2	Al_2O_3	Fe_2O_3	K_2O	MgO	CaO	Na_2O	SO_3

 doi:10.20944/preprints202602.0215.v1

Content (%)	62.55	22.94	5.158	3.151	1.90	1.31	1.22	0.206

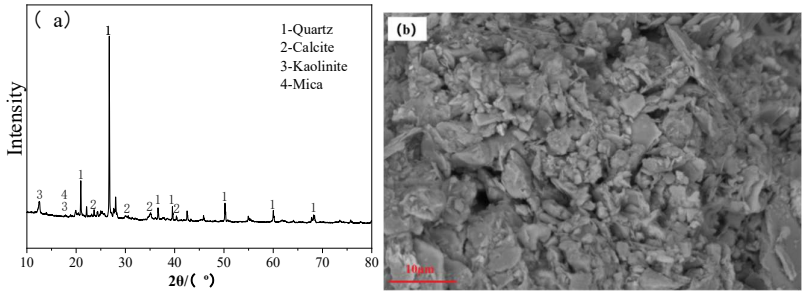

Figure 1. XRD pattern and micromorphology of CG: (a) XRD pattern; (b) SEM micrograph.

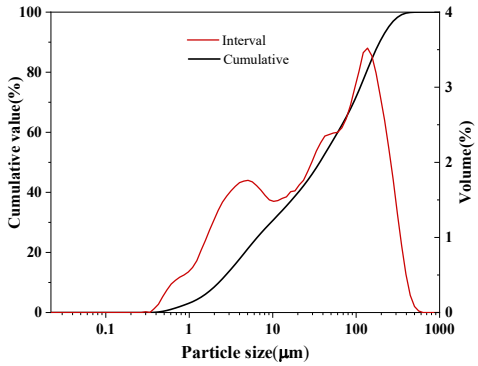

Figure 2. Particle size distribution curve of CG.

2.1.2. Activators

Three alkaline activators were employed: NaOH, $Ca(OH)_2$, and sodium silicate solution. NaOH and $Ca(OH)_2$ were analytical grade with 99% purity (Sinopharm Chemical Reagent Co., Ltd.). Sodium silicate had a modulus of 1.0 M, with SiO_2 content of 27.3% and Na_2O content of 8.54% (industrial grade, Shandong Silicate Co., Ltd.).

2.2. Experimental Procedure and Design

This study examined how different alkali activators influence CG cementitious performance. Three activators, $Ca(OH)_2$, NaOH, and sodium silicate, were tested at varying dosages. Compressive strength measurements were used to evaluate the activation efficiency. The experimental procedure and mix proportions are presented in Figure 3 and Table 2, respectively.

Figure 3. Experimental flow chart.

 doi:10.20944/preprints202602.0215.v1

Table 2. Mix proportions for CG cementitious performance tests.

Group	Sample ID	Alkali Activator Type	CG (g)	Activator Dosage (%)	W/B Ratio
1	0	-	300	0	0.3
2	Ca-5	$Ca(OH)_2$	300	5.0	0.3
3	Ca-7	$Ca(OH)_2$	300	7.0	0.3
4	Ca-10	$Ca(OH)_2$	300	10.0	0.3
5	Ca-12	$Ca(OH)_2$	300	12.0	0.3
6	Na-5	NaOH	300	5	0.3
7	Na-7	NaOH	300	7	0.3
8	Na-10	NaOH	300	10	0.3
9	Na-12	NaOH	300	12	0.3
10	Si-5	Sodium silicate	300	5	0.3
11	Si-7	Sodium silicate	300	7	0.3
12	Si-10	Sodium silicate	300	10	0.3
13	Si-12	Sodium silicate	300	12	0.3

2.3. Test Methods

2.3.1. Particle Size Distribution Test

Laser particle size distribution tests were performed on CG, fly ash, slag, and cement using dry method measurement to avoid interference from water-soluble components. The test instrument was a Mastersizer 3000 laser particle size analyzer. An appropriate amount of powder was placed in the dry dispersion system, with dispersion pressure set at 0.2 MPa, 3 scans, using air as the dispersion medium, to determine the particle size distribution range (D10, D50, D90) and distribution curves. This test aimed to clarify the particle gradation characteristics of raw materials and provide basic data for analyzing the influence of powder specific surface area on alkali-activation reaction rate and geopolymer filling material performance.

2.3.2. Multi-element Analysis

Multi-element analysis of CG raw materials was performed Chemical analysis was conducted via XRF spectrometry. The test instrument was a PANalytical Axios X-ray fluorescence spectrometer. 5 g of powder was pressed into a 40 mm diameter disc sample using the boric acid edge pressing method (pressure 30 MPa, holding time 30 s). Detection parameters were set as reference[14]. Analyzed elements included major oxides and trace heavy metal oxides, aiming to clarify key chemical characteristics of raw materials such as silicon-aluminum ratio and calcium content, providing data support for revealing the material basis of alkali-activation reactions in blended systems and environmental risk assessment.

2.3.3. Preparation of Alkali-activated CG Specimens

CG raw material, water, and alkali activator were sequentially added to the cement mortar mixer pot, followed by slow mixing for 180 s, pausing for 10 s, then fast mixing for 180 s. The mixed alkali-activated material was transferred into 40-mm cubic steel molds, followed by mechanical vibration (30 s) for void elimination. After smoothing the surface, specimens underwent controlled curing (>90% RH, 20±1° C) in a humidity chamber, with performance testing conducted after curing for 3 d, 7 d, and 28 d respectively. Each group of experiments was performed in triplicate.

2.3.4. Compressive Strength Test

 doi:10.20944/preprints202602.0215.v1

Compressive strength was measured following Chinese standard GB/T 17671-1999 on a YAW-300B servo-controlled testing machine at a loading rate of 2.4 kN/s. The compressive strength (Rc) was determined using Equation (1):

$$R_c = F_c/A \quad (1)$$

where F_c represents the load applied at failure of the half-block specimen (N), and A represents the compressed area (mm^2).

2.3.5. XRD Analysis

Phase composition analysis of CG raw materials and specimens (ground into powder) was performed using a Bruker D8 Advance XRD. Parameters were adopted from prior work[14]. During analysis, the diffraction peak positions and intensities in the patterns were compared with standard phase databases (ICDD PDF-2 database) to determine the phases present in the samples.

2.3.6. SEM-EDS Analysis

Specimens were tested using an FEI Quanta 650 SEM coupled with a Bruker QUANTAX EDS spectrometer. Dried samples were cut into small pieces to form fresh fracture surfaces of approximately 0.5–1 cm^2, gold-sputtered, and then observed under the SEM combined with EDS analysis.

3. Results and Discussion

3.1. Compressive Strength Analysis

The compressive strength development patterns of CG cementitious materials with different alkali activators and different dosages are showed in Figure 4(a)–(c).

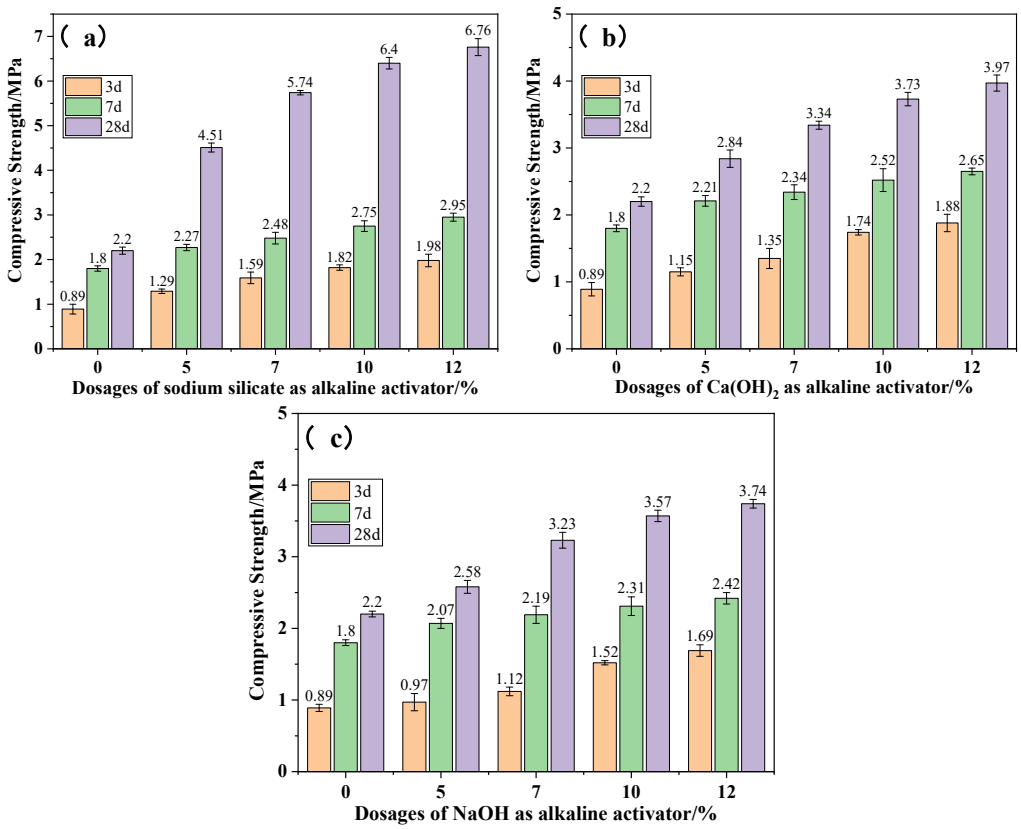

Figure 4. Effects of different alkali activators and dosages on compressive strength: (a) sodium silicate; (b) $Ca(OH)_2$; (c) NaOH.

 doi:10.20944/preprints202602.0215.v1

As shown in the figures, under the action of three different alkali activators, compressive strength exhibited a positive correlation with activator concentration. When specimens were cured for 28 d, the strength without alkali activator was 2.2 MPa. When the activator dosages were 5%, 7%, 10%, and 12%, the compressive strengths corresponding to sodium silicate were 4.51, 5.74, 6.4, and 6.76 MPa, with growth rates of 105.0%, 160.9%, 190.9%, and 207.3%, respectively; the compressive strengths corresponding to $Ca(OH)_2$ were 2.84, 3.34, 3.73, and 3.97 MPa, with growth rates of 29.09%, 51.82%, 69.55%, and 80.45%, respectively; the compressive strengths corresponding to NaOH were 2.58, 3.23, 3.57, and 3.74 MPa, with growth rates of 17.27%, 46.82%, 62.27%, and 70.00%, respectively.

The above results indicate the three activators exhibited markedly different activation capacities on CG, with efficiency ranking as: sodium silicate > $Ca(OH)_2$ > NaOH. This phenomenon can be explained from the perspective of alkali-activation reaction mechanism. Alkaline activators establish a high-pH milieu within the reaction matrix, where elevated OH^- concentrations disrupt the CG crystalline lattice, cleaving Si-O-Si and Si-O-Al linkages on mineral surfaces, dissolving inert silicon and aluminum into soluble monomers—silicate ions ($H_3SiO_4^-$/$H_2SiO_4^{2-}$) and aluminate ions ($Al(OH)_4^-$) [16]. Subsequently, Al^{3+} in aluminate ($Al(OH)_4^-$) replaces Si^{4+} in silicon-oxygen tetrahedra (SiO_4) to form negatively charged $[AlO_4]^{5-}$ structures. Monomers cross-link and polymerize through Si-O-Al and Si-O-Si bonds to form amorphous sodium (potassium) aluminosilicate gels (N-A-S-H gel), which can grow in interparticle gaps, reducing porosity, improving compactness, and increasing compressive strength [17,18].

At the same activator dosage, sodium silicate shows the most significant activation effect. At 10% activator dosage, the compressive strengths at 3 d, 7 d, and 28 d curing were 1.47, 1.84, and 1.72 times those of $Ca(OH)_2$, and 1.20, 1.19, and 1.79 times those of NaOH, respectively. Therefore, the advantage of sodium silicate is more significant at the same dosage. This is mainly because the hydrolysis of sodium silicate enhances the cementitious properties of CG through dual pathways: in addition to the OH^- generated enhancing system alkalinity to promote dissociation of silicon-aluminum phases in the CG system and release of active components, it also provides silicate ions (SiO_3^{2-}) as an external silicon source, which combines with dissolved aluminum species and sodium ions, forming dense cementitious structures dominated by hydrated sodium aluminosilicate (N-A-S-H) gel through condensation reactions [19,20]. To further verify the action mechanisms of the three activators, phase and microstructure analyses were performed.

3.2. Hydration Reaction Mechanism Analysis

3.2.1. Phase Composition Analysis

Figures 5(a) and (b) show the XRD patterns of sodium silicate, $Ca(OH)_2$, and NaOH at 5% dosage after 7 d and 28 d curing; Figures 5(c) and (d) show the XRD patterns of each activator at 10% dosage after 7 d and 28 d curing. First, the CG samples mainly contain mineral phases such as quartz, kaolinite, calcite, and mica. After alkali activation, phase changes occurred in all systems.

 doi:10.20944/preprints202602.0215.v1

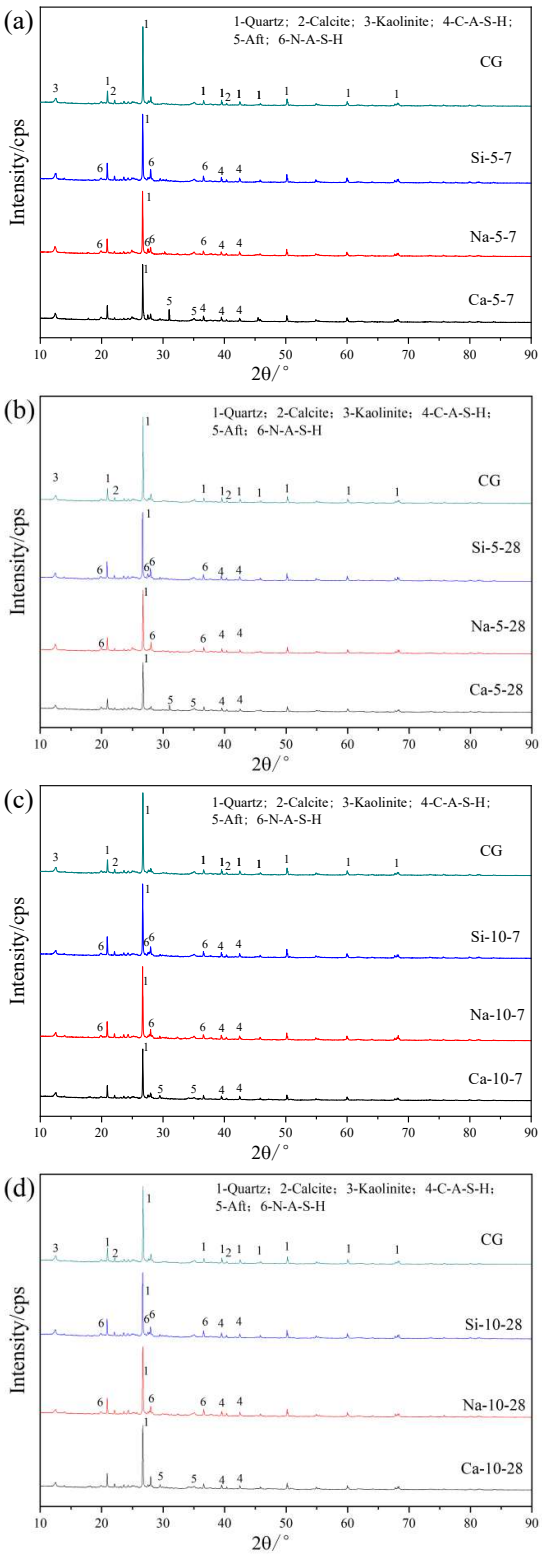

Figure 5. XRD patterns of CG with different alkali activators and dosages: (a) 5% dosage, 7 d curing; (b) 5% dosage, 28 d curing; (c) 10% dosage, 7 d curing; (d) 10% dosage, 28 d curing.

As can be seen from the figures, following alkaline treatment, quartz diffraction intensities diminished universally. Moreover, after activation of CG with sodium silicate and NaOH, novel N-A-S-H and C-A-S-H phases emerged; after activation with $Ca(OH)_2$, new phases AFt and C-A-S-H appeared. With increasing activator dosage, the diffraction peaks of cementitious products

 doi:10.20944/preprints202602.0215.v1

significantly increased. At 10% dosage, activation product peaks were stronger, original mineral (quartz, kaolinite) peaks were weaker, reactions were more complete, and gel phases (N-A-S-H, C-A-S-H) and AFt ($Ca(OH)_2$ activator) formation was more sufficient. According to Figures 5(a)–(d), different activator types affect product phases: sodium silicate and NaOH systems are dominated by N-A-S-H and C-A-S-H, exhibiting persistent accumulation over extended durations; $Ca(OH)_2$ activator, due to calcium ions, shows persistent prominent AFt peaks and enhanced C-A-S-H, reflecting its long-term contribution to ettringite and silicate gel [21]. Sodium silicate-activated samples show the most significant broadened diffuse peaks of N-A-S-H gel in the $2\theta = 10°–40°$ range [22–24] (Si-5-7, Si-5-28, Si-10-7, Si-10-28), with peak intensity significantly increasing with dosage, corresponding to the 28 d compressive strength growth rate of 207.3%, highly consistent with macroscopic mechanical properties. Therefore, the phase evolution results demonstrate that sodium silicate hydrolysis produces silicate and hydroxide ions, combining alkaline environment creation with active silicon supplementation, efficiently activating active silicon-aluminum components in CG and generating large amounts of amorphous cementitious products. In contrast, NaOH and $Ca(OH)_2$-activated samples have weak hydration product peaks, with inert phases (such as quartz) dominating, relying only on alkaline activation without active silicon supplementation, resulting in limited 28 d strength increases of 70.0% and 80.45%, respectively. This shows that sodium silicate has a dual activation effect, with its phase evolution highly consistent with macroscopic strength data, showing significant advantages in promoting cementitious product formation and improving later-age strength, while NaOH and $Ca(OH)_2$ have weaker effects due to their single activation mechanism relying only on alkaline activation. $Ca(OH)_2$ activator favors long-term AFt presence, while sodium silicate and NaOH activators dominate silicate gel accumulation, illustrating the long-term mineral phase evolution and activator regulation effects of alkali-activated materials.

3.2.2. Microstructure Analysis

Activation of CG Cementitious Properties by Sodium Silicate

Figures 6 and 7 show the SEM images of specimens at 5% and 10% sodium silicate dosage after 7 d and 28 d curing, respectively. As can be seen from Figure 6, at 5% sodium silicate dosage, CG hydration remained incomplete, yielding a porous microstructure, numerous cracks, and many unreacted particles. Extending curing time from 7 d to 28 d had limited effect on performance improvement, indicating that low-dosage sodium silicate failed to effectively promote the formation of dense gel networks. EDS spectra show that early hydration reaction products are mainly N-A-S-H gel, with Si/Al ratio ranging from 1.0 to 4.5, and very low calcium content (Ca/Si ≈ 0), indicating minimal calcium-based gel formation and weak alkaline environment (Figures 6(a) and (b)). At 28 d curing, C-A-S-H gel content slightly increased but was still insufficient to significantly improve structural compactness (Figures 6(c) and (d)).

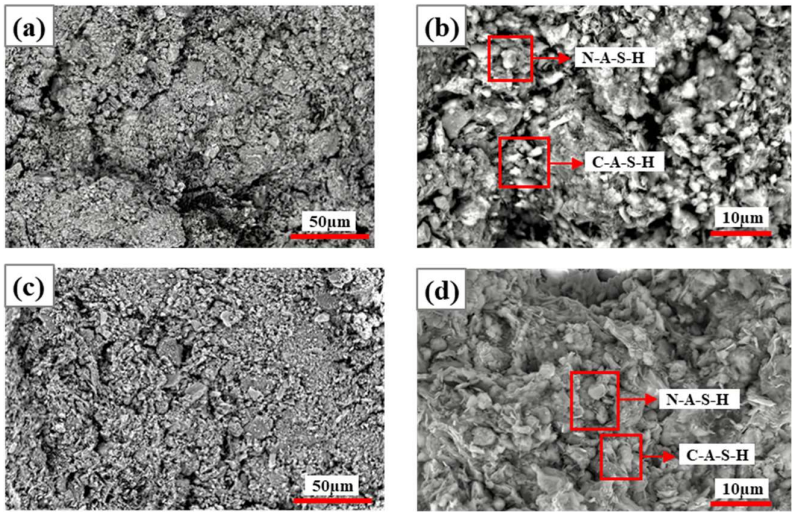

 doi:10.20944/preprints202602.0215.v1

Figure 6. SEM images of specimens with 5% sodium silicate at 7 d and 28 d curing: (a,b) 7 d curing; (c,d) 28 d curing.

In contrast, specimens at 10% sodium silicate dosage showed significantly enhanced compactness, reduced voids, and tight structure compared to 5% specimens with extended curing time. At 7 d curing (Figures 7(a) and (b)), N-A-S-H gel constituted the predominant hydration phase, with small amounts of C-A-S-H gel formed in local areas. At 28 d curing in later hydration reactions (Figures 7(c) and (d)), N-A-S-H and C-A-S-H became the dominant phases, calcium content significantly increased (15%–19%), Si/Al ratio stabilized at 6.0–8.0, and microstructural densification was markedly enhanced. Furthermore, Figure 7(d) shows that the two gels N-A-S-H and C-A-S-H are interconnected, indicating that they do not simply stack inside the solidified body but interact to jointly promote polymerization reactions in the system. This synergistic effect significantly improves solidification efficiency, thereby enhancing the mechanical properties of materials [25]. Therefore, sodium silicate dosage has a significant influence on CG geopolymerization reactions.

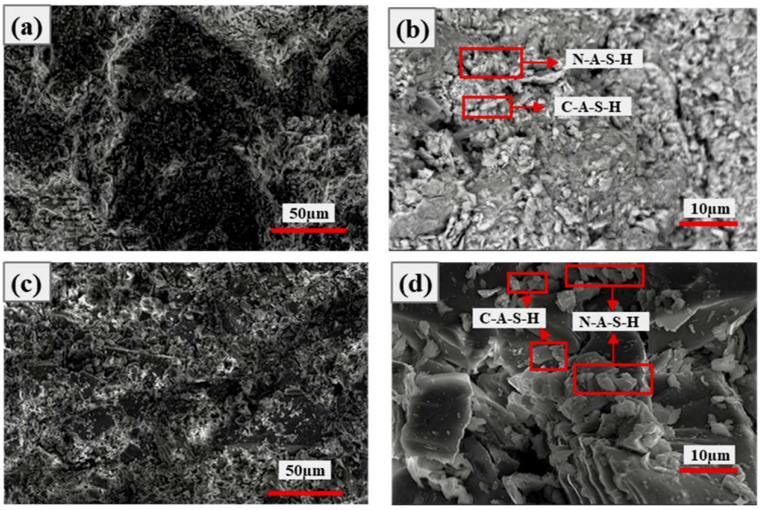

Figure 7. SEM images of specimens with 10% sodium silicate at 7 d and 28 d curing: (a,b) 7 d curing; (c,d) 28 d curing.

Activation of CG Cementitious Properties by $Ca(OH)_2$

Figures 8 and 9 show the SEM images of specimens at 5% and 10% $Ca(OH)_2$ dosage after 7 d and 28 d curing, respectively. As can be seen from Figure 8, at 5% $Ca(OH)_2$ dosage, the system structure was loose in early hydration (Figures 8(a) and (b)), with few hydration products, much residual $Ca(OH)_2$, small amounts of C-A-S-H gel, and limited aluminosilicate products. At 28 d curing (Figures 8(c) and (d)), structure was slightly denser, hydration products slightly increased, C-A-S-H gel was more typical, and AFt also formed, but overall reaction was slow, and according to EDS spectra, aluminum phase participation was limited.

 doi:10.20944/preprints202602.0215.v1

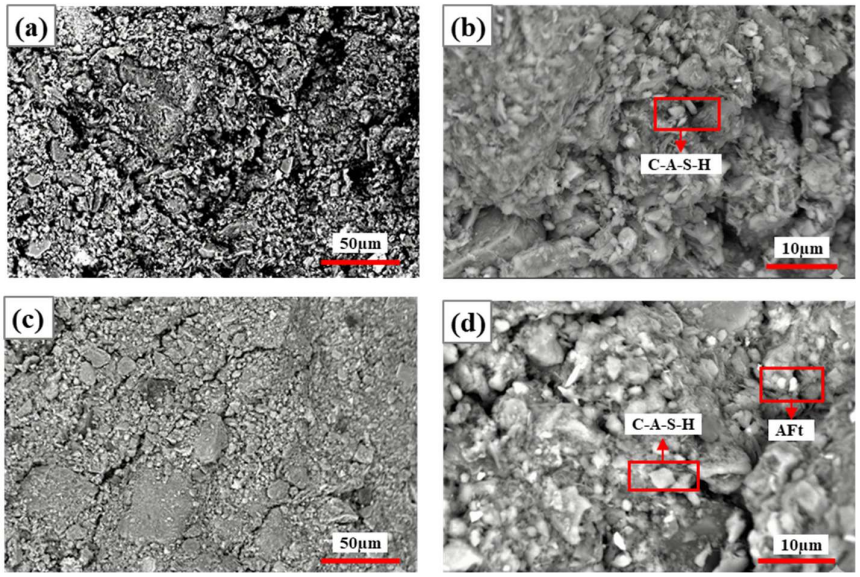

Figure 8. SEM images of specimens with 5% $Ca(OH)_2$ at 7 d and 28 d curing: (a,b) 7 d curing; (c,d) 28 d curing.

As can be seen from Figure 9, at 10% $Ca(OH)_2$ dosage, early hydration showed loose structure, poor uniformity, and few hydration products. With curing time extended to 28 d, structure became significantly dense, hydration products notably increased, C-A-S-H gel dominated the structure, and system cementitious properties improved. With the addition of alkaline activator, as curing time extended from 7 d to 28 d, all systems transformed from loose and porous to dense structures, hydration reactions became more complete, product types became richer, and in addition to AFt, $CaCO_3$ also appeared. These products jointly filled pores and improved structural stability, reflecting the time-dependent characteristics of $Ca(OH)_2$ activation of CG [26,27]. Meanwhile, prolonged curing is favorable for complete hydration reactions.

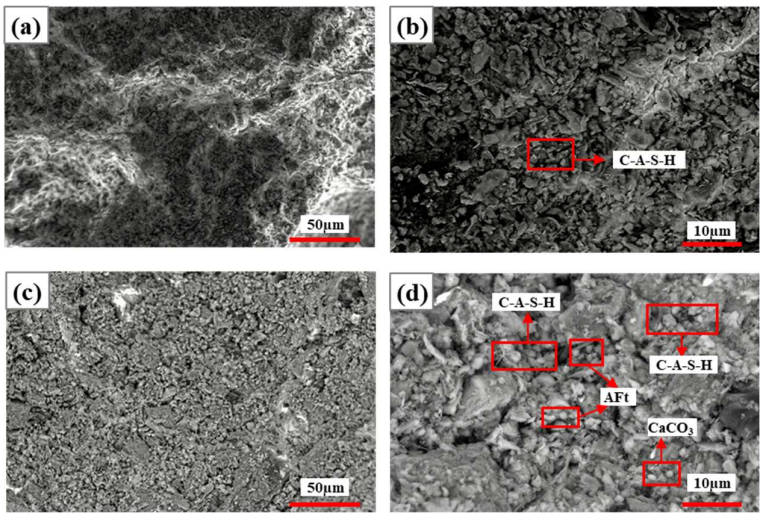

Figure 9. SEM images of specimens with 10% $Ca(OH)_2$ at 7 d and 28 d curing: (a,b) 7 d curing; (c,d) 28 d curing.

Activation of CG Cementitious Properties by NaOH

Figures 10 and 11 show the SEM images of specimens at 5% and 10% NaOH dosage after 7 d and 28 d curing, respectively. At 5% NaOH dosage, at 7 d curing (Figures 10(a) and (b)), early hydration showed rough specimen surfaces, irregular particles, and many pores; at 28 d curing (Figures 10(c) and (d)), structure was denser, large pores reduced, particles were tightly connected with network-like trends. At 5% NaOH dosage, according to EDS elemental ratios, at 7 d curing (Figure 10(b)), mainly N-A-S-H gel formed with limited calcium participation; at 28 d curing (Figure

 doi:10.20944/preprints202602.0215.v1

10(d)), silicon-based gel polymerization degree increased, Al incorporated, forming C-A-S-H gel, while more continuous N-A-S-H networks also formed, and sodium-rich N-A-S-H gel also appeared.

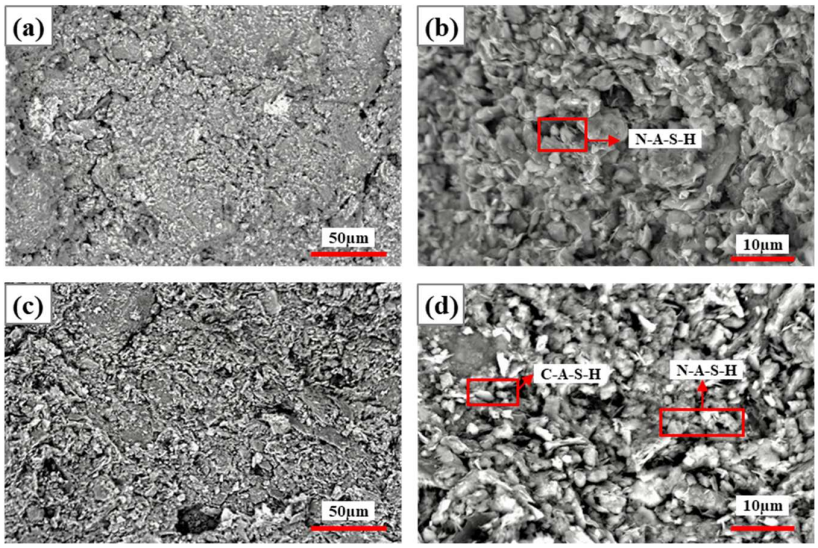

Figure 10. SEM images of specimens with 5% NaOH at 7 d and 28 d curing: (a,b) 7 d curing; (c,d) 28 d curing.

As shown in Figure 11, at 10% NaOH dosage, at 7 d curing (Figures 11(a) and (b)), particle aggregates were relatively dispersed, with later-stage structure further densifying and particle boundaries becoming blurred. Early alkali-activation reactions were intense, generating large amounts of N-A-S-H gel with little calcium-based mineral participation; at 28 d curing (Figures 11(c) and (d)), N-A-S-H gel still dominated, with Na/Si ratio at some EDS measurement points decreasing, gel structure transitioning to more stable networks, and silicon-aluminum polymerization degree increasing. In summary, with extended curing time, Na^+ utilization became more complete, developing from high-concentration Na^+-dominated gelation to multi-ion synergistic composite gel systems, with hydration reactions becoming more thorough. Meanwhile, microstructure transformed from loose packing to dense, element distribution became more uniform, and hydration product stability and cementing ability significantly improved.

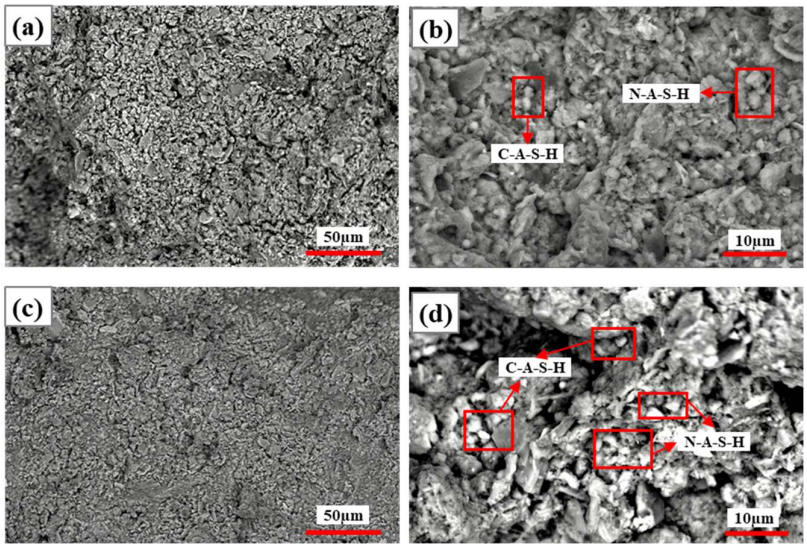

Figure 11. SEM images of specimens with 10% NaOH at 7 d and 28 d curing: (a,b) 7 d curing; (c,d) 28 d curing.

Integrating the SEM-EDS analysis results, the microstructure evolution patterns of the three activator systems can be summarized as follows: (1) Extended curing time promotes structural

 doi:10.20944/preprints202602.0215.v1

densification in all systems, but the sodium silicate system achieves the highest degree of densification; (2) Alkali activators destroy CG crystal structures by providing an alkaline environment (OH^-), causing Si-O-Si and Si-O-Al bond breakage, releasing soluble silicon-aluminum monomers ($H_3SiO_4^-$, $Al(OH)_4^-$), which then cross-link and polymerize through Si-O-Al and Si-O-Si bonds to generate cementitious products (N-A-S-H, C-A-S-H, AFt, etc.), filling interparticle gaps and reducing porosity, ultimately improving material strength. In the sodium silicate system, N-A-S-H and C-A-S-H gels develop synergistically; in the $Ca(OH)_2$ system, C-A-S-H dominates accompanied by AFt; while the NaOH system is dominated by N-A-S-H; (3) 10% sodium silicate activator dosage combined with 28 d curing is the optimal condition for achieving sufficient reaction and structural densification.

4. Conclusions

(1) In terms of macroscopic properties, both activator chemistry and concentration exert strong control over strength development of CG specimens. With increasing alkali activator dosage (5%–12%), specimen compressive strength shows an increasing trend. Among them, sodium silicate has the best activation effect, with compressive strength reaching 6.4 MPa at 10% dosage after 28 d curing, a growth rate of 190.9%; $Ca(OH)_2$ and NaOH have weaker activation effects, with strength growth rates of 69.55% and 62.27%, respectively, under the same conditions. The efficiency ranking of the three activators is: sodium silicate > $Ca(OH)_2$ > NaOH. Experimental results indicate that 10% sodium silicate dosage combined with 28 d curing is the optimal condition.

(2) Microstructure and phase evolution results further confirm the macroscopic property patterns. XRD analysis shows that sodium silicate-activated samples exhibit significant broadened diffuse peaks of N-A-S-H gel in the $2\theta = 10°–40°$ region, with peak intensity increasing with dosage, while original mineral (quartz, kaolinite) peak intensities weaken, reflecting more complete reactions, with with N-A-S-H gel serving as the primary binding phase; $Ca(OH)_2$ activator, due to calcium ions, generates yielding C-A-S-H gel alongside substantial AFt precipitation (ettringite), but overall cementitious product quantity is lower; NaOH activator mainly generates N-A-S-H gel, but its peak intensity is weaker than the sodium silicate system.

(3) SEM-EDS analysis reveals the microscopic mechanisms of hydration reactions: at low dosage (5%) alkali activator, CG reaction degree is low, structure is loose, with many unreacted particles, and gel products are dominated by N-A-S-H (sodium silicate, NaOH systems) or C-A-S-H ($Ca(OH)_2$ system); at high dosage (10%) with extended curing time (28 d), system structure significantly densifies—in sodium silicate-activated samples, C-A-S-H and N-A-S-H gels act synergistically; in $Ca(OH)_2$ system, C-A-S-H and $CaCO_3$ (carbonation product) jointly fill pores; in NaOH system, N-A-S-H gel network becomes more continuous—all demonstrating the promoting effect of "high dosage + prolonged curing" on reaction deepening. Sodium silicate, with its dual function of alkaline activation and active silicon supplementation, shows significant advantages in promoting CG activation.

Author Contributions: Conceptualization, Chao Geng,Quanming Li and Yajie Gao; Writing—original Draft Preparation, Yajie Gao, Chao Geng, Yilin Heng; Writing—Review and Editing, Quanming Li, Chao Geng, Xianfeng Shi, and Kai Han; Visualization, Wei Li, Cheng Chen, Hong Zhang and Yukai Wang; Supervision,Quanming Li and Zongyuan Mao.

Funding: This work was supported by the Outstanding Young Scientist Program Project of Beijing Universities (No.JWZQ20240101017), the Key Science and Technology Program of the Ministry of Emergency Management of China No. 2025EMST080201).and the Scientific Research Foundation for North China University of Technology (No. 11005136025XN076-051).

References

1. National Bureau of Statistics of China. China Statistical Yearbook 2023; China Statistics Press: Beijing, China, 2025.

 doi:10.20944/preprints202602.0215.v1

2. Wu, H.; Chen, C.; Song, W.; et al. Toward sustainable construction: Comprehensive utilization of coal gangue in building materials. J. Build. Eng. 2025, 99, 111556.
3. Li, Q.M.; Geng, C.; Zhang, H.; Shi, X.F.; Liu, J.G.; Chen, C. The large-scale sustainable utilization status of bauxite residue (red mud): Challenges and perspectives for China. Environ. Rev. 2025, 33, 1–16.
4. Li, J.; Wang, J. Comprehensive utilization and environmental risks of coal gangue: A review. J. Clean. Prod. 2019, 239, 117946.
5. Zhang, Y.L.; Ling, T.C. Reactivity activation of waste coal gangue and its impact on the properties of cement-based materials—A review. Constr. Build. Mater. 2020, 234, 117424.
6. Zheng, Q.W.; Zhou, Y.; Liu, X.; et al. Environmental hazards and comprehensive utilization of solid waste coal gangue. Prog. Nat. Sci. Mater. Int. 2024, 34, 223–239.
7. Zhou, W.; Chen, S.; Ouyang, J.; et al. Effects of the silicate modulus of water glass on the hydration and mechanical properties of alkali-activated blast furnace ferronickel slag. Front. Mater. 2021, 8, 748833.
8. Wang, X.; Liu, F.; Li, L.; et al. Study on the compressive strength and reaction mechanism of alkali-activated geopolymer materials using coal gangue and ground granulated blast furnace slag. Materials 2024, 17, 3659.
9. Zhang, L.; Zhang, Y.; Wang, Q.; et al. Sustainable alkali-activated materials: Leveraging spontaneous combustion coal gangue for enhanced cementitious performance. Mater. Today Commun. 2024, 41, 111044.
10. Feng, D.; Wang, J.; Wang, Y.; Xiao, X.; Hou, W.; Liang, S. Alkali-activated geopolymer materials prepared from coal gangue and municipal solid waste incineration byproducts. J. Build. Eng. 2024, 82, 108285.
11. Zhao, J.; Wang, A.G.; Zhu, Y.C.; et al. Manufacturing ultra-high performance geopolymer concrete (UHPGC) with activated coal gangue for both binder and aggregate. Compos. Part B Eng. 2024, 284, 111723.
12. Lv, X.; Qin, Y.; Lin, Z.; et al. Effect of an alkali activators on the compressive strength and reaction mechanism of coal gangue-slag-fly ash geopolymer grouting materials. Constr. Build. Mater. 2024, 426, 136154.
13. Provis, J.L.; Bernal, S.A. Geopolymers and related alkali-activated materials. Annu. Rev. Mater. Res. 2014, 44, 299–327.
14. Geng C, Chen C, Shi X, Wu S, Jia Y, Du B, Liu J. Recovery of metals from municipal solid waste incineration fly ash and red mud via a co-reduction process. Resources, Conservation and Recycling, 2020,154: 104600.
15. Lu, T.; Li, Z.; Huang, H. Structural evolution of calcium sodium aluminosilicate hydrate (C-(N-)A-S-H) gels induced by water exposure: The impact of Na leaching. Cem. Concr. Res. 2024, 178, 107453.
16. Guo, Y.; Zhao, Q.; Yan, K. High-capacity utilization of coal gangue as supplementary cementitious material, geopolymer, and aggregate: A review. Constr. Build. Mater. 2024, 411, 134731.
17. Zhu, H.; Liang, G.; Li, H.; et al. A multiscale study on gel composition of hybrid alkali-activated materials partially utilizing air pollution control residue as an activator. Cem. Concr. Compos. 2023, 136, 104898.
18. Myers, R.J.; Bernal, S.A.; San Nicolas, R.; et al. Generalized structural description of calcium-sodium aluminosilicate hydrate gels: The cross-linked substituted tobermorite model. Langmuir 2013, 29, 5294–5306.
19. Wang, X.; Liu, F.; Pan, Z.; et al. Geopolymerization of coal gangue via alkali-activation: Dependence of mechanical properties on alkali activators. Buildings 2024, 14, 787.
20. Ma, H.Q.; Zhu, H.G.; Yi, C.; et al. Preparation and reaction mechanism characterization of alkali-activated coal gangue-slag materials. Materials 2019, 12, 2250.
21. Li, Z.; Lu, T.; Liang, X.; et al. Mechanisms of autogenous shrinkage of alkali-activated slag and fly ash pastes. Cem. Concr. Res. 2020, 135, 106107.
22. Dong, W.; Li, W.; Guo, Y.; et al. Compressive and Flexural Properties of Ultra-Fine Coal Gangue-Based Geopolymer Gels and Microscopic Mechanism Analysis. Polymers 2022, 14, 1537.
23. Su, L.J.; Yang, J.B. Application research of alkali activated coal gangue based geopolymer in the field of engineering materials. In Proceedings of the HCCE 2024; Atlantis Press: Paris, France, 2025; pp. 601–607.
24. Zhu, H.; Yang, S.; Li, W.; et al. Study of Mechanical Properties and Durability of Alkali-Activated Coal Gangue-Slag Concrete. Materials 2020, 13, 5576.
25. Walkley, B.; San Nicolas, R.; Sani, M.A.; et al. Examination of alkali-activated material nanostructure during thermal treatment. J. Mater. Sci. 2018, 53, 9486–9503.

 doi:10.20944/preprints202602.0215.v1

26. Puertas, F.; Palacios, M.; Manzano, H.; et al. A model for the C-A-S-H gel formed in alkali-activated slag cements. J. Eur. Ceram. Soc. 2011, 31, 2043–2056.
27. Ben Haha, M.; Le Saout, G.; Winnefeld, F.; et al. Influence of activator type on hydration kinetics, hydrate assemblage and microstructural development of alkali activated blast-furnace slags. Cem. Concr. Res. 2011, 41, 301–310.